Electronic Supplementary Material (ESI) for Physical Chemistry Chemical Physics.

Modelling Aqueous Solubility of Sodium Chloride in Clays at Thermodynamic Conditions of Hydraulic Fracturing by Molecular Simulations SUPPLEMENTARY INFORMATION

Filip Moučka,[1,2] Martin Svoboda,[1,2] and Martin Lísal[1,2]

[1] *Laboratory of Aerosols Chemistry and Physics, Institute of Chemical Process Fundamentals of the CAS, v. v. i., Prague, Czech Republic*

[2] *Department of Physics, Faculty of Science, J. E. Purkinje University, Ústí n. Lab., Czech Republic*

*Corresponding author: lisal@icpf.cas.cz

Mailing address: Laboratory of Aerosols Chemistry and Physics, Institute of Chemical Process Fundamentals of the Czech Academy of Sciences, v. v. i., Rozvojová 135/1, 165 02 Prague 6-Suchdol, Czech Republic

S1 Chemical Potentials and Solubility in the Bulk Solution

Our intention is to study a confined aqueous electrolyte solution in equilibrium with a saturated solution in a bulk reservoir at a temperature of $T_{\rm bulk}$ and a pressure of $P_{\rm bulk}$, corresponding to a typical shale gas reservoir condition of 365 K and 275 bar [1]. Hence, it is necessary to evaluate the values of the chemical potentials for NaCl and water, $\mu_{\rm NaCl}$ and $\mu_{\rm H_2O}$, at $T_{\rm bulk}$, $P_{\rm bulk}$ and the concentration (expressed by molality, m) equal to the salt solubility in the bulk phase, $m_{\rm bulk}$, where $m_{\rm bulk}$ is also unknown and needs to be determined as well.

We calculated the dependence of $\mu_{\rm NaCl}$ and $\mu_{\rm H_2O}$ on m by the Osmotic Ensemble Monte Carlo (OEMC) method [2, 3]. The OEMC method is similar to the Grand Canonical Monte Carlo (GCMC) method outlined in the main text. In the OEMC method, the bulk solution is simulated at fixed $P_{\rm bulk}$, $T_{\rm bulk}$, values of chemical potential of a set of species, and numbers of particles of the remaining species. The numbers of particles for species, whose chemical potentials are specified, fluctuate during OEMC simulations, utilising the expanded ensemble procedure identical to that in the expanded ensemble GCMC. We performed two sets of the simulations: (i) for the determination of the $\mu_{\rm NaCl}(m)$ curve, where the number of the ions fluctuates at specified values of $\mu_{\rm NaCl}$ and a fixed number of water molecules, and (ii) for the calculation of the $\mu_{\rm H_2O}(m)$ curve, where the number of water molecules fluctuates at specified $\mu_{\rm H_2O}$ and a fixed number of the ions. The range of the inputting values of $\mu_{\rm NaCl}$ and $\mu_{\rm H_2O}$ were chosen based on our previous works [2, 3, 4].

The output from the OEMC simulations involves equilibrium concentrations at specified values of chemical potentials. These data can be approximated by analytical formulas, originally developed for the correlation of experimental chemical potential data [5] and lately also used in the molecular simulation studies [6, 7, 8], i.e.,

$$\mu_{\rm NaCl} = \mu^{\dagger}_{\rm NaCl} + 2RT\ln m + 2RT\ln(10)\left(-\frac{A\sqrt{m}}{1+B\sqrt{m}} + bm + Cm^2 + Dm^3\right) \tag{S1}$$

$$\mu_{\rm H_2O} = \mu^{*}_{\rm H_2O} - 2RTmM_{\rm H_2O} - RTM_{\rm H_2O}\ln(10) \times\left(bm^2 + \frac{4}{3}Cm^3 + \frac{3}{2}Dm^4 + \frac{2A}{B^3+B^4\sqrt{m}} + \frac{4A\ln(B\sqrt{m}+1)}{B^3} - \frac{2A\sqrt{m}}{B^2} - \frac{2A}{B^3}\right) \tag{S2}$$

where R is the universal gas constant, T is the temperature, and $\mu^{\dagger}_{\rm NaCl}$, $\mu^{*}_{\rm H_2O}$, A, B, b, C,

and D are adjustable parameters. The adjustable parameters are further related via the Gibbs-Duhem equation [6], leaving only five fitting parameters. In addition, the value of A can be expressed using the dielectric constant of the water model, κ, as [9, 10]

$$A = \frac{1.824 \cdot 10^6}{(\kappa T)^{3/2}} \tag{S3}$$

We calculated the dielectric constant via a molecular simulation of pure water in either isobaric-isothermal or canonical ensembles. The rest of the parameters were obtained by minimising the sum of squares of the deviations of simulated equilibrium concentrations from the approximation functions (S1) and (S2). In principle, A can be also treated as an adjustable parameter which results in larger uncertainty of the fit at low concentrations [6].

In order to find the solubility value in the bulk phase, we calculated the chemical potential of crystalline salt, $\mu_{\mathrm{NaCl}}(\mathrm{s})$, by the Frenkel-Ladd method [11]. We simulated the crystal of NaCl in periodic boundary conditions employing a different number of ions to minimise finite-size effects, and extrapolated the results of $\mu_{\mathrm{NaCl}}(\mathrm{s})$ to the thermodynamic limit. The solubility is then determined as the concentration at which $\mu_{\mathrm{NaCl}}(\mathrm{s}) = \mu_{\mathrm{NaCl}}$, where μ_{NaCl} is given by Eq. (S1). Therefore as the inputting chemical potentials to the GCMC simulations of the clay systems, we used a value of $\mu_{\mathrm{NaCl}}(\mathrm{s})$ for μ_{NaCl} and a value of $\mu_{\mathrm{H_2O}}$ obtained from Eq. (S2) at the calculated solubility.

In addition, we also considered confined solutions in equilibrium with the bulk solution at 365 K and 275 bar, and a concentration corresponding to the experimental solubility, $m^{\mathrm{se}}_{\mathrm{bulk}} = 6.6$ kg/mol, at 365 K and 1 bar [12]. The inputting chemical potentials μ_{NaCl} and $\mu_{\mathrm{H_2O}}$ are then given by Eqs. (S1) and (S2), respectively, evaluated at $m^{\mathrm{se}}_{\mathrm{bulk}}$.

S2 Simulation Details

In both the GCMC and OEMC simulations, we split the insertion/deletion of a water molecule to five sub-processes of different λ values and the change of the NaCl amount to 15 such sub-processes (cf. Eq. (4) in the main text), and we used $R_s = 2.5$ Å. In the GCMC simulations, we employed a spherical cut-off $R_c = 8.9$ and 12 Å for pyrophyllite and Na-montmorillonite (Na-MMT), respectively, and neglected the corresponding long-range tail corrections. In the OEMC, we used the standard spherical cut-off $R_c = 9$ Å and the tail corrections for homogeneous bulk systems [13]. We treated the electrostatic interactions by the standard Ewald summation (ES) method [13, 14] since the supercells employ periodic boundary conditions in all three directions, and we used the value of the Ewald screening parameter $\alpha = \pi/R_c$. No dipole corrections were employed to compensate for the symmetry of the slit pore. We further utilised $15 \times 15 \times 91$ and $15 \times 27 \times 91$ vectors in the reciprocal space for the pyrophyllite and Na-MMT supercells, respectively, and $15 \times 15 \times 15$ vectors in the OEMC simulations. In the GCMC, we selected different Monte Carlo (MC) steps randomly with probabilities of 0.1, 0.1, 0.3, and 0.5 corresponding to a change of the numbers of the particles, translation of an ion, translation of a water molecule, and rotation of a water molecule, respectively. In the OEMC at a fixed number of water molecules, we used the probabilities of 0.004, 0.1, 0.1, 0.496, and 0.3 for a volume change, a change of the number of the ions, translation of a fractional ion, translation of a fully-interacting ion, and rotation of a water molecule. In the OEMC at a fixed number of ions, we utilised the probabilities of 0.004, 0.1, 0.1, 0.1, 0.396, 0.3 for a volume change, a change of number of water molecules, translation of a fractional water molecule, rotation of a fractional water molecule, translation of a fully-interacting water molecule, and rotation of a fully-interacting water molecule. Typically, about 7×10^9 MC steps were attempted during the OEMC and GCMC simulations.

Molecular dynamics (MD) simulations were performed with the LAMMPS code [15], employing a spherical cut-off $R_c = 12$ Å. In the MD simulations, we treated the long-range electrostatic interactions by the particle-particle particle-mesh (PPPM) algorithm [16] with a precision of $1 \cdot 10^{-4}$ [17]. We further used a time step of 1 fs and the MD simulations were typically run for 2 ns.

For the pyrophyllite, we found that the use of the slab geometry gives the same results as use of the supercell set-up. In our slab-geometry set-up, two parallel walls separated by

a distance H formed a slit, and the individual periodic images of the slit were separated by a distance of 100 Å in the z-direction. For the slab geometry, we employed the standard ES or PPPM techniques with the Yeh-Berkowitz correction [18].

S3 Results for the Bulk Phase

The simulation results for the chemical potentials of NaCl and water, μ_{NaCl} and $\mu_{\mathrm{H_2O}}$, and the density of aqueous NaCl solution, ρ_s, as a function of concentration, m, at a temperature of 365 K and a pressure of 275 bar are shown in Fig. S1. Besides the simulation data, we also plot the approximation curves corresponding to Eqs. (S1) and (S2) with the fitting parameters listed in Table S1, and a cubic polynomial regression curve representing the values of ρ_s. The values of the chemical potentials used in this work were considered with respect to the ideal-gas standard chemical potentials corresponding to the standard Gibbs free energy of formation in the NIST-JANAF thermochemical tables [19]: $\mu^0_{\mathrm{Na^+}} = 566.417$ kJ/mol, $\mu^0_{\mathrm{Cl^-}} = -241.440$ kJ/mol, and $\mu^0_{\mathrm{H_2O}} = -225.543$ kJ/mol at a temperature of 365 K.

In Fig. S1, the $\mu_{\mathrm{NaCl}}(m)$ curve exhibits an increasing concave behaviour which continuously changes from a logarithmic dependence at low concentrations to almost linear dependence at high concentrations. Similar behaviour was observed in previous studies at different thermodynamic conditions, see e.g. Refs. [4, 8, 10]. The $\mu_{\mathrm{H_2O}}(m)$ curve is also concave over the entire range of concentrations, and its decreasing dependence on concentration is weaker when compared with the $\mu_{\mathrm{NaCl}}(m)$ curve. Use of the Frenkel-Ladd method resulted in the value of the chemical potential of crystalline NaCl, $\mu_{\mathrm{NaCl}}(\mathrm{s}) = -376.30$ kJ/mol, which is indicated by the dashed horizontal line in $\mu_{\mathrm{NaCl}}(m)$ portion of Fig. S1. At the intersection of $\mu_{\mathrm{NaCl}}(\mathrm{s})$ with the $\mu_{\mathrm{NaCl}}(m)$ curve, the solid and liquid phases are in an equilibrium and the value of the solubility in the bulk phase, $m^{\mathrm{sm}}_{\mathrm{bulk}} = 3.14_3$ mol/kg, can be found on the molality axis, and is indicated by the first of the two solid vertical lines. The intersections of this vertical line with the $\mu_{\mathrm{H_2O}}(m)$ and $\rho_s(m)$ curves then yield, respectively, the chemical potential of water, $\mu_{\mathrm{H_2O}} = -229.12$ kJ/mol, and the density of the saturated solution, $\rho_s = 1082.6_5$ kg/m^3. For the GCMC simulations of clay pores in equilibrium with the bulk reservoir of a concentration of 6.6 mol/kg (supersaturated phase with respect to the model, and indicated by the second vertical line in Fig. S1), the inputting μ_{NaCl} and $\mu_{\mathrm{H_2O}}$ are given by Eqs. (S1) and (S2) and they equal to -368.58 kJ/mol and -229.78 kJ/mol, respectively. In addition, $\rho_s = 1175.0_5$ kg/m^3 was obtained from the $\rho_s(m)$ curve of Fig. S1.

A value of the chemical potential for water at zero concentration was obtained by a set of OEMC simulations with zero ion pairs and the value of inputting $\mu_{\mathrm{H_2O}}$ varied from

-229.1 to -228.5 kJ/mol. The interval corresponds to the vicinity of an extrapolated value of μ_{H_2O} to zero concentration as obtained by Eq. (S2). Such OEMC simulations never reach an equilibrium and the number of water molecules either continuously increases or decreases. The value of μ_{H_2O} at zero concentration then corresponds to a turning point between cases with increasing and decreasing numbers of water molecules. Such an approach was used in our previous work and yields results with relatively small statistical uncertainty of the chemical potential for pure water [20].

We also verified our OEMC methodology by (i) reproducing published simulation results at different thermodynamic conditions [10] and (ii) simulating the NaCl chemical potential using the Multi-Stage Free Energy Perturbation (MSFEP) method [4]; see also Fig. S1. As evident from Fig. S1, the results either agree within statistical uncertainties with the published simulation results [10] or they are consistent within statistical uncertainties with MSFEP results.

The value of parameter A reported in Table S1 was obtained using Eq. (S3) and a value of water dielectric constant, κ, from isobaric-isothermal MC simulation at T_{bulk} and P_{bulk}. The simulated κ was then verified by MC simulation in a canonical ensemble using the fluctuation formula

$$\kappa = 1 + \frac{\langle M^2 \rangle}{3\epsilon_0 V k T_{\text{bulk}}} \tag{S4}$$

In Eq. (S4), M is the magnitude of the total electric dipole moment of the bulk solution in a simulation box with the volume V, ϵ_0 is the permittivity of free space, and k is the Boltzmann constant. Kolafa and Viererblová [21] have shown that Eq. (S4) can be efficiently used when the saturation of polarization is in the range from 0.05 to 0.1. In our simulation, the value of the saturation is 0.088 and the simulations result in $\kappa = 52.45_1$.

Table S1: Values of the adjustable parameters of Eqs. (S1) and (S2) which approximate the simulated chemical potentials for NaCl and water at a temperature of 365 K and a pressure of 275 bar.

$\mu^{\dagger}_{\mathrm{NaCl}}$ (kJ/mol)	$\mu^{*}_{\mathrm{H_2O}}$ (kJ/mol)	A	B	b	C	D
-386.882	-228.696	0.688600	10.2001	0.204537	-0.0183305	0.00103520

Table S2: Water content, n_{H_2O}, ion concentrations, m_{Na^+} and m_{Cl^-}, interlayer fluid energy, u, and density of the aqueous NaCl solution, ρ_s, adsorbed into the pyrophyllite slits of the width H as obtained by Grand Canonical Monte Carlo simulations. The confined solution is in equilibrium with the bulk solution of a salt concentration of 3.14 mol/kg at a temperature of 365 K and a pressure of 275 bar. $n_{H_2O} = 1000 N_{H_2O} M_{H_2O} / m_{clay}$, where N_{H_2O} is the number of water molecules in the slit, $M_{H_2O} = 18.0153$ g/mol is the molecular mass of water and $m_{clay} = 11529.85$ g/mol is the mass of a simulation slit wall used. $m_{Na^+} = m_{Cl^-} \equiv m = N_i / (N_{H_2O} M_{H_2O})$, where N_i are the numbers of Na^+ and Cl^- in the slit, respectively. The simulation uncertainties are given in the last digits as subscripts.

H (Å)	n_{H_2O} (mg_{H_2O}/g_{clay})	m (mol/kg)	u (kJ/mol)	ρ_s (kg/m^3)
8	~ 0.1	~ 0	~ 0	~ 0.2
9	107.0_{21}	0.64_{41}	-32.1_{10}	632.8_{129}
10	120.7_{24}	0.89_{37}	-37.3_{11}	651.6_{130}
12	158.1_{32}	1.54_{34}	-49.2_{15}	736.9_{147}
14	192.6_{39}	1.74_{33}	-53.8_{16}	778.2_{156}
16	229.2_{46}	1.93_{32}	-57.6_{17}	818.2_{164}
18	264.5_{53}	2.21_{28}	-61.9_{19}	851.4_{170}
20	298.2_{60}	2.33_{30}	-64.0_{19}	869.6_{174}
22	336.1_{67}	2.14_{27}	-62.7_{19}	882.3_{176}
24	370.8_{74}	2.41_{24}	-66.1_{20}	904.6_{181}
26	405.3_{81}	2.71_{22}	-69.9_{21}	926.9_{185}
28	443.1_{85}	2.56_{20}	-68.6_{21}	933.8_{195}

Table S3: Water content, n_{H_2O}, ion concentrations, m_{Na^+} and m_{Cl^-}, interlayer fluid energy, u, and density of the aqueous NaCl solution, ρ_s, adsorbed into the Na-montmorillonite slits of the width H as obtained by Grand Canonical Monte Carlo simulations. The confined solution is in equilibrium with the bulk solution of a salt concentration of 3.14 mol/kg at a temperature of 365 K and a pressure of 275 bar. $n_{H_2O} = 1000 N_{H_2O} M_{H_2O} / m_{clay}$, where N_{H_2O} is the number of water molecules in the slit, $M_{H_2O} = 18.0153$ g/mol is the molecular mass of water and $m_{clay} = 23008.42$ g/mol is the mass of a simulation slit wall used. $m_{Na^+} = N_{Na^+} / (N_{H_2O} M_{H_2O})$ and $m_{Cl^-} = N_{Cl^-} / (N_{H_2O} M_{H_2O})$, where N_{Na^+} and N_{Cl^-} are the numbers of Na^+ and Cl^- in the slit, respectively. The simulation uncertainties are given in the last digits as subscripts.

H (Å)	n_{H_2O} (mg_{H_2O}/g_{clay})	m_{Na^+} (mol/kg)	m_{Cl^-} (mol/kg)	u (kJ/mol)	ρ_s (kg/m^3)
7	78.3_{17}	6.66_{21}	~ 0	-92.7_{19}	662.4_{119}
8	99.2_{20}	5.34_{18}	0.09_{4}	-84.5_{17}	716.8_{134}
9	117.3_{24}	4.55_{17}	0.11_{7}	-78.9_{16}	741.9_{142}
10	134.8_{23}	4.11_{15}	0.24_{11}	-76.1_{15}	763.3_{148}
12	170.9_{34}	3.84_{16}	0.79_{15}	-75.9_{15}	816.1_{162}
14	205.5_{41}	3.93_{16}	1.39_{15}	-78.5_{16}	859.3_{169}
16	240.9_{49}	3.72_{26}	1.55_{26}	-77.5_{16}	881.4_{176}
18	276.9_{56}	3.52_{23}	1.63_{23}	-76.4_{15}	899.5_{179}
20	312.1_{63}	3.52_{20}	1.85_{20}	-77.2_{15}	919.1_{183}
22	347.0_{70}	3.50_{18}	1.99_{18}	-77.4_{15}	932.3_{187}
24	382.6_{77}	3.43_{17}	2.07_{16}	-77.2_{15}	943.3_{188}
26	417.9_{85}	3.43_{15}	2.18_{15}	-77.5_{16}	954.4_{189}
28	454.9_{91}	3.16_{14}	1.97_{14}	-74.6_{15}	952.4_{191}

Table S4: Water content, n_{H_2O}, ion concentrations, m_{Na^+} and m_{Cl^-}, interlayer fluid energy, u, and density of the aqueous NaCl solution, ρ_s, adsorbed into the Na-montmorillonite slits of the width H as obtained by Grand Canonical Monte Carlo simulations. The confined solution is in equilibrium with the bulk solution of a salt concentration 6.6 mol/kg at a temperature of 365 K and a pressure of 275 bar. $n_{H_2O} = 1000 N_{H_2O} M_{H_2O}/m_{clay}$, where N_{H_2O} is the number of water molecules in the slit, $M_{H_2O} = 18.0153$ g/mol is the molecular mass of water and $m_{clay} = 23008.42$ g/mol is the mass of a simulation slit wall used. $m_{Na^+} = N_{Na^+}/(N_{H_2O} M_{H_2O})$ and $m_{Cl^-} = N_{Cl^-}/(N_{H_2O} M_{H_2O})$, where N_{Na^+} and N_{Cl^-} are the numbers of Na^+ and Cl^- in the slit, respectively. The simulation uncertainties are given in the last digits as subscripts.

H (Å)	n_{H_2O} (mg_{H_2O}/g_{clay})	m_{Na^+} (mol/kg)	m_{Cl^-} (mol/kg)	u (kJ/mol)	ρ_s (kg/m^3)
9	113.3_{23}	5.73_{33}	1.12_{28}	-90.0_{18}	755.3_{138}
14	194.8_{35}	6.20_{35}	3.52_{34}	-99.9_{20}	905.4_{177}
20	293.9_{59}	6.28_{23}	4.51_{23}	-103.0_{21}	984.1_{202}
26	391.1_{78}	6.39_{25}	5.05_{25}	-105.1_{21}	1024.5_{243}

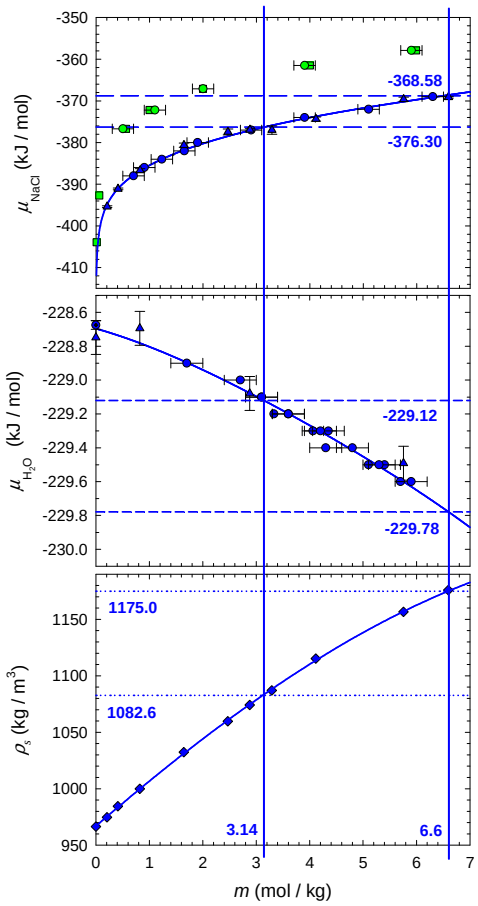

Figure S1: Simulation results of the bulk NaCl aqueous solution at a temperature of 365 K and a pressure of 275 bar. The chemical potential for NaCl, μ_{NaCl}, as a function of concentration, m. The chemical potential for water, $\mu_{\mathrm{H_2O}}$, as a function of m. The solution density, ρ_s, as a function of m. Key: circles, Osmotic Ensemble Monte Carlo (OEMC) simulations; triangles, Multi-Stage Free Energy Perturbation simulations; diamonds, isobaric-isothermal Monte Carlo simulations; green squares, published simulations of Mester and Panagiotopoulos at a temperature of 473.15 K and a pressure of 15.5 bar [10]; green circles, comparison of our OEMC simulations with Mester and Panagiotopoulos' simulations. The solid lines in the first and second portions of the figure correspond to the approximation curves given by Eqs. (S1) and (S2) with the adjustable parameters listed in Table S1. The solid line in the third portion of the figure represents a cubic polynomial fit to ρ_s data. The horizontal lines indicate the properties of the bulk solution with the value of the NaCl concentration denoted by the vertical solid lines.

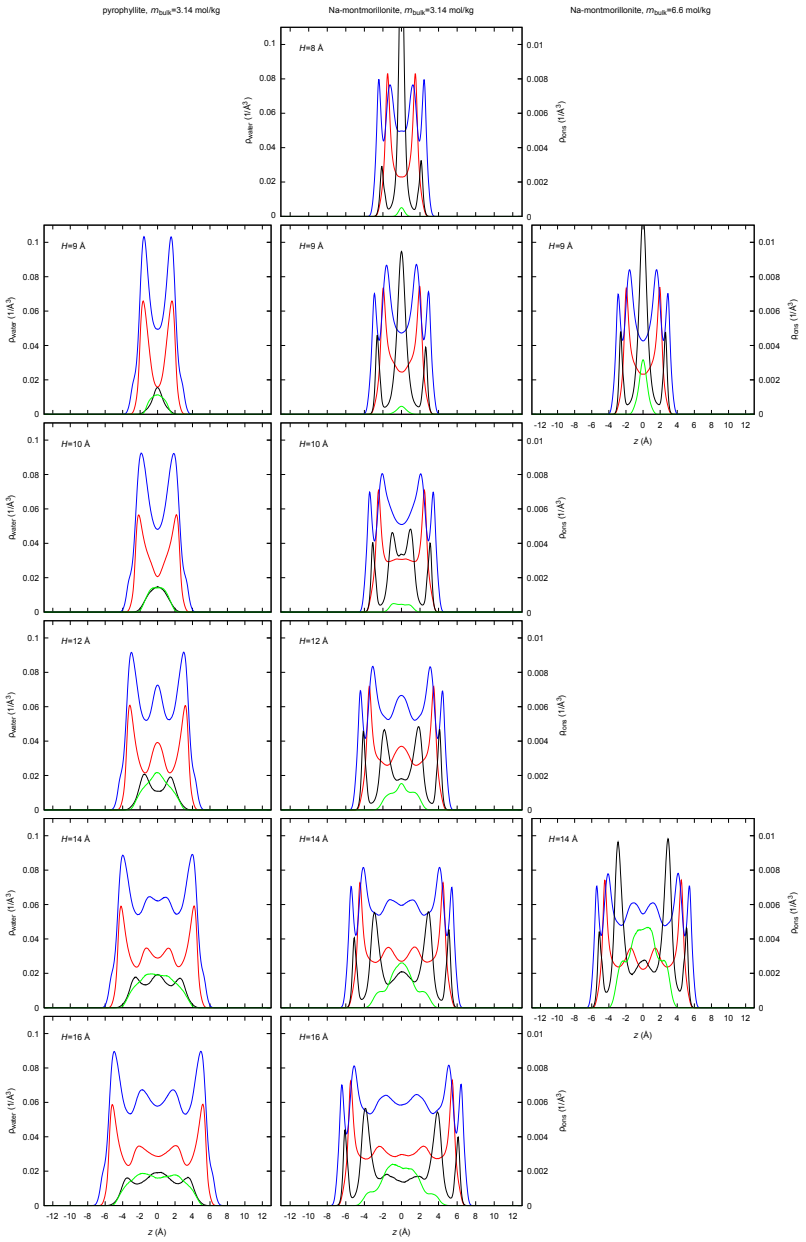

Figure S2: The atomic density profiles, $\rho_\alpha(z)$, for the pyrophyllite and Na-montmorillonite in equilibrium with the bulk solution of the salt concentrations 3.14 and 6.6 mol/kg at a temperature of 365 K and a pressure of 275 bar, showing interlayer ions, Na^+ (black) and Cl^- (green), water oxygen (red), and water hydrogen (blue). $H = \{8, 9, 10, 12, 14, 16\}$ Å is the slit width and z is the distance of a particle from the centre of the slit which is located at $z = 0$.

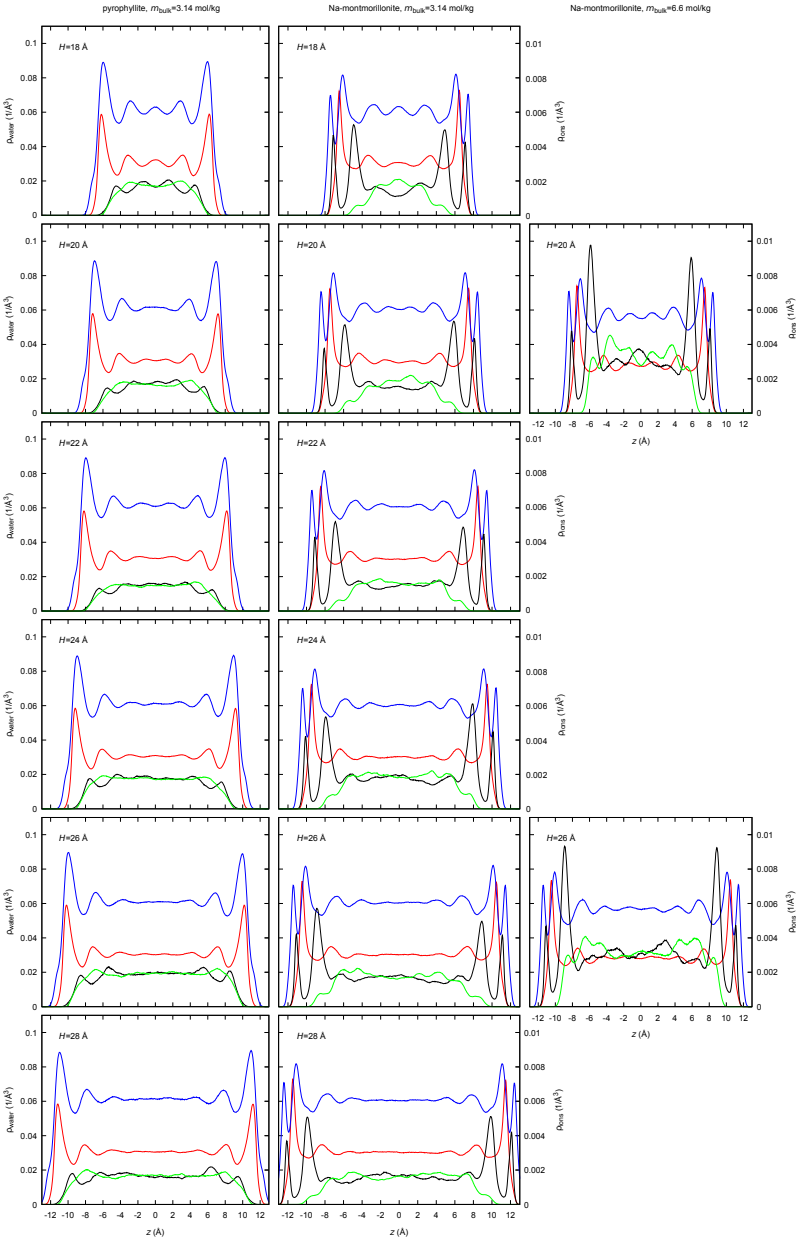

Figure S3: The atomic density profiles, $\rho_\alpha(z)$, for the pyrophyllite and Na-montmorillonite in equilibrium with the bulk solution of the salt concentrations 3.14 and 6.6 mol/kg at a temperature of 365 K and a pressure of 275 bar, showing interlayer ions, Na^+ (black) and Cl^- (green), water oxygen (red), and water hydrogen (blue). $H = \{18, 20, 22, 24, 26, 28\}$ is the slit width and z is the distance of a particle from the centre of the slit which is located at $z = 0$.

References

[1] K. A. Bullin and P. E. Krouskop, *Oil & Gas J.* 2009, **107**, 50-55.

[2] M. Lísal, W. R. Smith, and J. Kolafa, *J. Phys. Chem. B* 2005, **109**, 12956-12965.

[3] F. Moučka, M. Lísal, J. Škvor, J. Jirsák, I. Nezbeda, and W. R. Smith, *J. Phys. Chem. B* 2011, **115**, 7849-7861.

[4] F. Moučka, M. Lísal, and W. R. Smith, *J. Phys. Chem. B* 2012, **116**, 5468-5478.

[5] W. J. Hamer and Y. C. Wu, *J. Phys. Chem. Ref. Data* 1972, **1**, 1047-1099.

[6] F. Moučka, I. Nezbeda, and W. R. Smith, *J. Chem. Phys.* 2013, **139**, 124505.

[7] F. Moučka, I. Nezbeda, and W. R. Smith, *Molec. Simul.* 2013, **39**, 1125-1134.

[8] Z. Mester and A. Z. Panagiotopoulos, *J. Chem. Phys.* 2015, **142**, 044507.

[9] C. W. Davies, *J. Chem. Soc.* 1938, 2086- 2093.

[10] Z. Mester and A. Z. Panagiotopoulos, *J. Chem. Phys.* 2015, **143**, 044505.

[11] D. Frenkel and A. J. C. Ladd, *J. Chem. Phys.* 1984, **81**, 3188-3193.

[12] H. Stephen and T. Stephen, *Solubilities of Inorganic and Organic Compounds*, Macmillan: New York, 1963.

[13] M. P. Allen and D. J. Tildesley, *Computer Simulation of Liquids*, Clarendon Press: Oxford, UK, 1987.

[14] D. Frenkel and B. Smit, *Understanding Molecular Simulation. From Algorithms to Applications*, Elsevier: Amsterdam, The Netherlands, 2002.

[15] S. J. Plimpton, *J. Comput. Phys.* 1995, **117**, 1-19.

[16] R. W. Hockney and J. W. Eastwood, *Computer Simulation Using Particles*, Adam Hilger: NY, 1989.

[17] J. Kolafa and J. W. Perram, *Molec. Simul.* 1992, **9**, 351-368.

[18] C. Yeh and M. L. Berkowitz, *J. Chem. Phys.* 1999, **111**, 3155-3162.

[19] M. Chase Jr., *NIST-JANAF Thermochemical Tables; Journal of Physical and Chemical Reference Data Monograph No. 9*, American Chemical Society and American Institute of Physics: Woodbury, NY, 1998.

[20] F. Moučka, I. Nezbeda, and W. R. Smith, *J. Chem. Theory Comput.* 2015, **11**, 1756-1764.

[21] J. Kolafa and L. Viererblová, *J. Chem. Theory Comput.* 2014, **10**, 1468-1476.